Supplement of Atmos. Chem. Phys., 16, 12703–12713, 2016
http://www.atmos-chem-phys.net/16/12703/2016/
doi:10.5194/acp-16-12703-2016-supplement

Atmospheric Chemistry and Physics Open Access EGU

Supplement of

Photolysis of frozen iodate salts as a source of active iodine in the polar environment

Óscar Gálvez et al.

Correspondence to: Óscar Gálvez (oscar.galvez@csic.es, oscar.galvez@ccia.uned.es)

1. Description of the Experiments

The table S1 shows the conditions of generation, irradiation and water proportion for all samples studied in this paper. The rate constant values, calculated as the slope of the best linear fit of the representation of natural logarithm of the integrated band intensities of an specific IR band versus time (see eq E3 in the manuscript), are also included for the five band analysed. The mean value of the different rate constants and the standard deviation are also shown in this table.

The band at 1430 cm^{-1} is the most suitable to follow the photolysis process, as it has been discussed in the MS, nevertheless, it can also be observed by monitoring the decay of the IO_3^- band (at 740 cm^{-1}), although due to the overlapping of water adsorptions this band is more difficult to be integrated and quantified. In any case, and when the water proportion is low, both bands show similar rate constant values (taken into account the error intervals and the corrections needed to take into account the dependence of 1:0.75 between both bands mentioned in the main MS), as it is shown in table S1. In addition, the decay of the band at 2844 cm^{-1} (ascribed to NH_4^+ stretching adsorptions) follows also a similar rate than those previously mentioned, which finally yields a similar rate constant value. As in the case of the 740 cm^{-1} band, water adsorptions disturb the integration of the 2844 cm^{-1} band, which is the main reason for the absence of values for several samples in the table. Furthermore, a growing band at approx. 2227 cm^{-1} is observed during the irradiation process, which is ascribed to a product formation (it could belong to molecules presenting N-O bonds). This band shows also a similar rate of intensity variation (see table). However, this affirmation should be taken with caution, due to, in most of the samples, the growing rate of this band cannot be fitted with a first order kinetic, so a more complicated process could be occurred. Finally, the band at 1300 cm^{-1} shows a considerable higher rate of variation, around three times faster, than the previous bands. This band belongs to a product of the photolysis reaction (again it could be ascribed to molecules presenting N-O bonds), but the different rate observed could be explained by several contributions from different products to this bands or considering a contribution from a single molecule which could be formed in a ratio 3:1 with respect to IO_3^- or NH_4^+ ions.

In the calculation of the J value of the photolysis process, we have taken into account only the rate constant values for the 1430 and 740 cm^{-1} bands. For the last one, the rate values at low temperatures it should be corrected by a factor of 1:0.75 due to this is the dependence

between these two bands at Tª ≤ 200 K (see manuscript for details). The averaged value for the photolysis rate in this study is J = (4±2) x 10^{-5} s^{-1}.

Table S1. List of the conditions of generation and irradiation of the samples analysed.

Nº Exp	T dep. IO_3^-	T dep. H_2O	H_2O dep.[a]	T Irrad.	IO_3^-:H_2O ratio	k (1430)[b]	k (740)[b]	k (1300)[b]	k (2227)[b]	k (2844)[b]
1	180	180	*HQ*	180	3.1 : 1	-4,00	-4,58	---	---	---
2	200	200	*HQ*	200	5 : 1	-5,18	-3,25	---	---	---
3	200	200	*HQ*	200	8.4 : 1	-2,55	-2,17	4,45	---	-2,95
4	200	200	*HQ*	200	6.2 : 1	-5,73	-4,10	13,45	1,73	-5,05
5	200	200	*HQ*	200	1 : 3.2	-3,83	-2,60	12,78	---	-3,05
6	200	200	*HQ*	200	3 : 1	-3,52	-2,32	10,07	---	-3,15
7	200	200	*HQ*	200	6.4 : 1	-3,13	-2,27	5,02	10,92	-1,88
8	150	150	*HQ*	150	5.3 : 1	-2,62	-1,83	10,85	2,25	-2,72
9	150	150	*HQ*	150	4.5 : 1	-3,93	-2,43	9,93	2,73	-4,67
10	298	298	*HQ*	298	15.1 : 1	-2,67	-2,70	---	---	-3,15
11	100	100	*HQ*	100	1 : 4	-3,00	---	7,45	2,18	-4,13
12	100	100	*HQ*	100	7.8 : 1	-4,63	-3,22	13,10	7,87	-4,37
13	100	100	*HQ*	100	2.1 : 1	-1,82	---	6,77	2,50	-4,62
14	253	253	*HQ*	253	1.6 : 1	-2,05	-1,95	10,78	---	-1,52
15	200	200	*HQ*	200	5.6 : 1	-2,05	-3,72	14,28	2,40	-5,70
16	100	100	*HQ*	100	1 : 80	-5,83	---	13,07	---	-4,28
17	100	100	*HQ*	100	1 : 15	-3,17	---	14,15	---	-2,55
18	140	140	*HQ*	140	1 : 8	-3,33	---	12,53	---	---
19	200	140	*Vap*	140	1 : 9	-5,08	---	8,30	---	---
20	215	100	*Vap*	100	1 : 1.9	-2,32	---	7,03	2,90	-6,90
21	260	140	*Vap*	140	1 : 1	-1,38	---	15,07	7,37	-5,82
22	200	200	*HQ*	200	8.4 : 1	-5,32	-3,23	7,08	4,12	-7,02
23	200	200	*HQ*	200	7.6 : 1	-4,97	-3,92	7,97	---	-9,33
					Mean	*-3,6*	*-3,0*	*10,2*	*5,0*	*-4,4*
					SD[c]	*1,3*	*0,8*	*3,3*	*3,9*	*2,0*

[a] *HQ* or *Vap* refer to hyperquenching or vapour deposited techniques respectively. [b] *k* values x 10^5 in s^{-1} (negative values are for reactants decays and positive for the appearance of products). [c] Standard Deviation of the J values calculated in the experiments.

2. Calculation of the spectral irradiance received by the samples.

To calculate the irradiance received by the samples, we have taken into account the lamp spectrum provided by the manufacturer, see Fig S1.

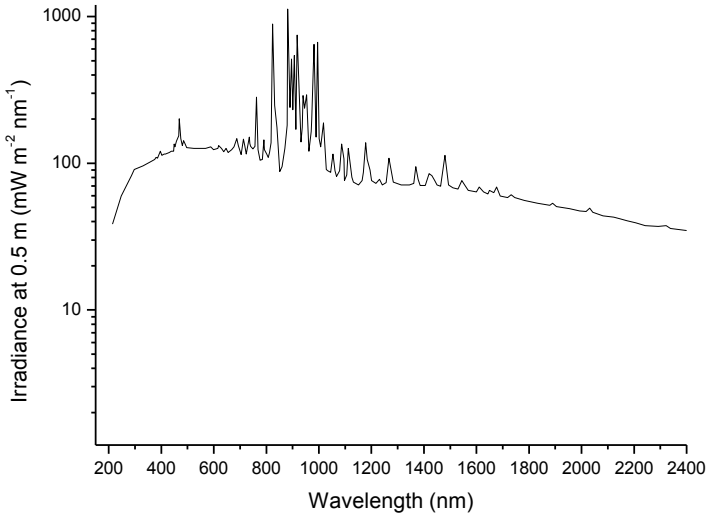

Figure S1. Irradiance spectra of the 1000 W LOT® Xenon Arc lamp.

This spectrum extends only to 2400 nm but the thermopile cover a wider range to approx. 11000 nm (11μm). To estimate the contribution of the radiation from 2400 to 11000 nm, we have simulated our spectrum by that of a blackbody at a temperature of around 5800 K (which fits to the solar spectrum). In this case, more than 95 % of the intensity radiation is emitted below 2400 nm, so contribution of radiation above 2400 nm can be practically ignored (or simply corrected our data by 0.95) in the calculation of the irradiance of the lamp.

The next step is integrating the spectrum of the lamp from 250 nm (which is the blue-side cut-off of our glass window, see main MS) to a certain red-limit (for example, 400 nm), and then calculate the percentage of the radiation received by the sample at the selected wavelength interval. In this integration, we have taken into account the UV-Vis spectra of the glass window of the chamber (see Fig. 2 of the main manuscript), which shows that the transmittance of the window changes from practically zero at 250 nm to almost 100 % at 350 nm, so the integration of this area (from 250 to 350 nm) has been corrected to account this feature. The calculation was carried out resulting in a value of 6.3 % of the total lamp power that entries in the chamber belong to the wavelength interval from 250 to 400 nm.

The average thermopile reading is 1.5 W cm^{-2}, which is substantially higher than the usual solar irradiance at the surface (at mid-latitude) around 0.1 W cm^{-2} (Houghton, 2002).

Since we know the irradiance spectra of the lamp, the percentage of radiation in the selected interval that penetrates in the chamber and the average thermopile reading during experiments, we can calculate the irradiance received in the samples in the wavelengths interval from 250 to 400 nm, which results of approx. 0.095 W cm^{-2}. This power can be compared by the solar irradiance at the surface in this wavelength interval, which can be estimated assuming a blackbody spectral distribution of a total irradiance of 0.1 W cm^{-2}. This calculation for the blackbody distribution results in 0.011 W cm^{-2} from 250 to 400 nm. Consequently, the substrate was irradiated with an average light power (at the relevant interval from 250 to 400 nm) of around 8 times higher than that registered in the Earth´s surface at mid-latitude. However, our silica substrate is highly reflecting to visible light, so due to the irradiation occurs perpendicularly to the substrate, probably our samples receive the double of flux (incident and reflected) than that above calculated. Even more reflexions are not discarded. Finally, two times the calculated value (0.19 W) has been estimated as the total flux in the interval from 250 to 400 nm received by the samples along the experiments.

3. First tests on the photolysis of iodinated frozen solutions.

In Figure S2, we show the photolysis process for KIO_3/H_2O ice mixture (initially with a 4 : 1 ratio) in comparison with NH_4IO_3/H_2O ice mixture (5.3 : 1 ratio). As it can be seen in the figure, the photolysis also occurs for KIO_3 ices samples, although the *J* value obtained for these experiments were smaller, between 3 to 8 times lower than the measured mean value for NH_4IO_3 experiments. Nevertheless, these initial tests were done without installing the thermopile, and therefore the focus of the solar lamp was not properly aligned, so presumably the irradiance received by KIO_3 samples was considerable lower than in NH_4IO_3 experiments.

After these initial tests with KIO_3, in order to follow the photolysis process preventing the overlapping of water and IO_3^- bands (in addition of other problems mentioned in the main manuscript), we finally chose NH_4IO_3 salt for the complete study of the photolysis of iodated frozen solutions.

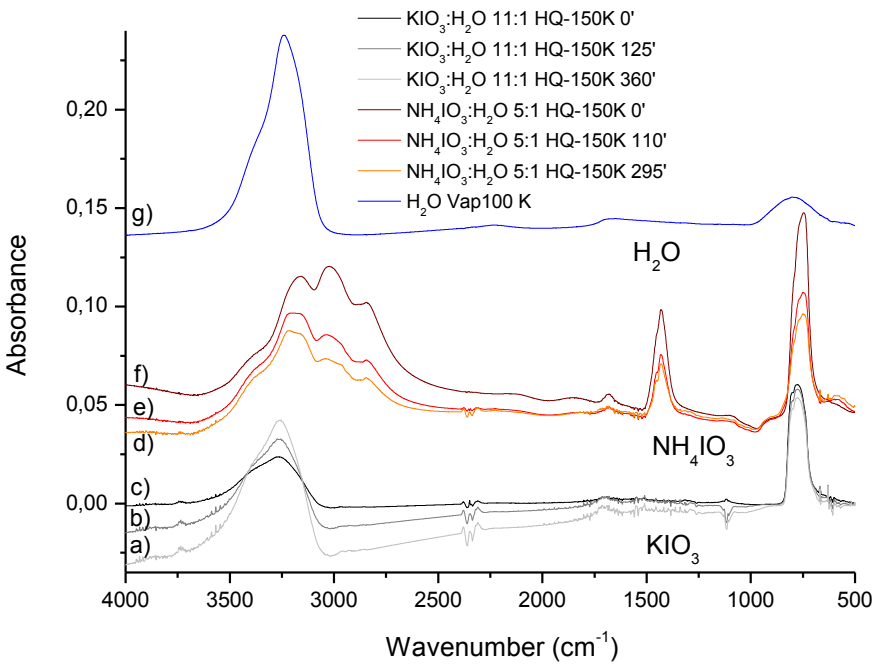

Figure S2. Evolution of the mid-IR transmission spectra of a 5:1 NH_4IO_3:H_2O and 4:1 KIO_3:H_2O deposited by HQ technique at 150 K during photolysis at that temperature. Water spectrum is also included for comparison purpose.

4. Calculations of the integrated absorption coefficient for IO_3^-

For IO_3^-, we are not aware of previous data in the literature of the integrated value of the IR absorption coefficient (A value) for the 740 cm^{-1} band, so, in this case, we have estimated this value for our most dried samples (to avoid the overlapping of the H_2O band) at t=0 (before photolysis). The mean value of the ratio of integration of 740 and 1300 cm^{-1} bands is 2.46 ± 0.12.

For the NH_4^+, we select the A(1400)= 4.0 x 10^{-17} cm $molec^{-1}$, so A (740) can be calculated as: 2.46 x 4.0 x 10^{-17} cm $molec^{-1}$ = (9.8 ± 0.5) x 10^{-17}. The error has been calculated taking into account two times the standard deviation.

Table S2. Integrated band values of the 1430 and 740 cm^{-1} bands for several samples studied.

T Dep	NH_4^+:H_2O ratio	Int $1430_{t=0}$	Int $740_{t=0}$	Int$(740)_{t=0}$/Int$(1430)_{t=0}$	HQ or VP
180	3.1 : 1	3,502	1,54518	2,266	HQ
200	5 : 1	9,363	3,712	2,522	HQ
200	4.2 : 1	2,3238	0,92812	2,504	HQ
200	8.4 : 1	6,92	2,9407	2,353	HQ
200	6.2 : 1	8,523	3,7908	2,248	HQ
200	1 : 3.2	4,97	1,99	2,497	HQ
200	3 : 1	3,64	1,5	2,427	HQ
200	6.4 : 1	12,2	4,97	2,455	HQ
150	5.3 : 1	8,4942	3,4913	2,433	HQ
150	4.1 : 1	8,1498	3,1415	2,594	HQ
150	4.5 : 1	5,8442	2,2388	2,610	HQ
100	1 : 4	5,579	2,131	2,618	HQ
100	7.8 : 1	7,59	3,124	2,430	HQ
200	5.6 : 1	4,3503	1,7314	2,513	HQ
260	1.4 : 1	8,0671	3,2308	2,497	Vap
260	1 : 1	7,552	2,87976	2,622	Vap
200	8.4 : 1	12,31	5,347	2,302	HQ
200	7.6 : 1	9,402	4,092	2,298	HQ

5. Absorption Cross Section of NH_4IO_3 solutions.

The UV-Vis spectra from 190 to 500 nm of diluted samples at different concentrations of NH_4IO_3 salt have been measured. The spectra are shown in Figure S3.

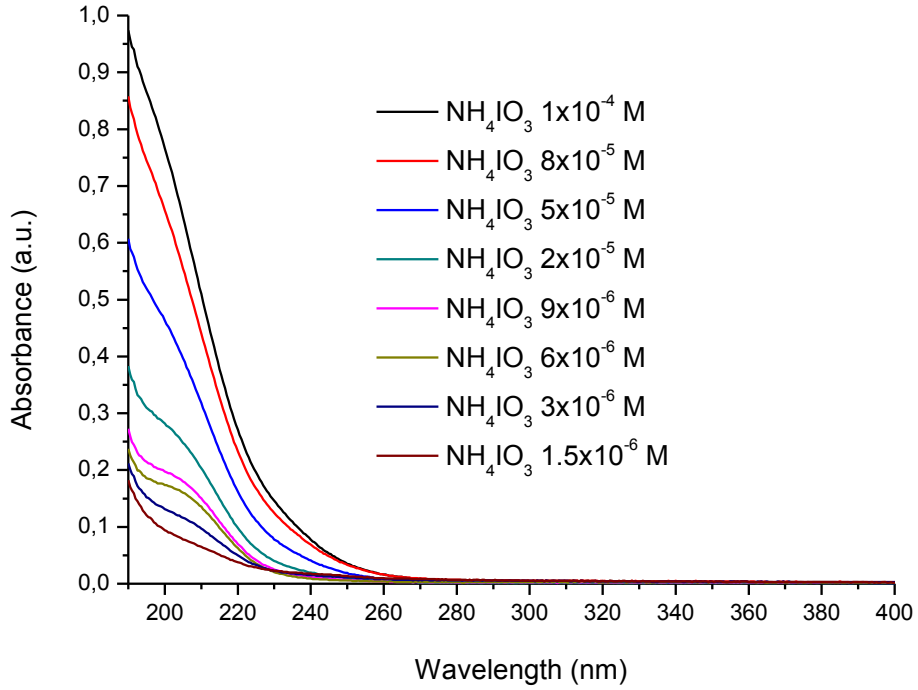

Figure S3. UV-Vis absorption spectra from 190 to 400 nm for different concentrations of NH_4IO_3 aqueous solutions (in absorbance unit).

A linear regression of the absorbance values from the different solutions versus concentration at different wavelengths gives a slope equal to the molar absorptivity at the corresponding wavelength. If the molar absorptivity is given in L mol^{-1} cm^{-1}, the cross section (in cm^2 $molec^{-1}$) is calculated via the equation:

$$\sigma = \frac{\varepsilon * \ln(10) * 1000}{N_A}$$

Following this procedure, the molar absorptivity and the cross section values have been calculated from 190 to 400 nm. The data are collected in Table S3 and a representation of the absorption cross section is shown in the Figure 6 in the main MS.

As can be seen in Fig S3, the absorbance above 290 nm is very low, and the errors in the calculated slope are large (Table S3). To evaluate the wavelength interval where the absorption cross section values measured are meaningful, in Fig. S4 we have plotted the

natural log of the cross section vs. wavelength, which in many case follow a straight line (see. e.g. (Twardowski et al., 2004). As can be observed in this figure, points beyond 290 nm deviate from the linear fit. This together with the large errors in the absorption cross sections, indicates that can be considered as noise. To avoid it, we have extrapolated these values to that obtained by the line provided by the best linear fitting of the points in the 200-290 nm interval. The absorption cross sections values using this correction are shown in the right column of Table S3. These new values have been used for the rest of calculations (quantum yield, action spectra and for the input of the atmospheric model).

Table S3. Molar Absorptivity and cross sections values for a liquid solution of NH_4IO_3 in the interval from 190 to 400nm.

Wavelength[a]	Molar absorptivity[a]	Error[a]	Cross Section[a]	Cross Section extrap[b]
190	8050	204	3,08E-17	3,08E-17
195	7456	179	2,85E-17	2,85E-17
200	6588	225	2,52E-17	2,52E-17
205	5476	239	2,09E-17	2,09E-17
210	4258	209	1,63E-17	1,63E-17
215	3162	138	1,21E-17	1,21E-17
220	2303	61	8,81E-18	8,81E-18
225	1718	21	6,57E-18	6,57E-18
230	1314	37	5,03E-18	5,03E-18
235	982	46	3,75E-18	3,75E-18
240	692	47	2,65E-18	2,65E-18
245	452	44	1,73E-18	1,73E-18
250	281	39	1,08E-18	1,08E-18
255	183	31	6,99E-19	6,99E-19
260	107	31	4,09E-19	4,09E-19
265	72	28	2,77E-19	2,77E-19
270	41	26	1,57E-19	1,57E-19
275	25	25	9,61E-20	9,61E-20
280	20	22	7,47E-20	7,47E-20
285	15	21	5,76E-20	5,76E-20
290	9	21	3,56E-20	4,53E-20
295	15	17	5,63E-20	2,96E-20
300	5	15	2,06E-20	2,03E-20
305	7	13	2,66E-20	1,39E-20
310	5	12	1,82E-20	9,51E-21
315	13	10	4,99E-20	6,52E-21
320	6	13	2,41E-20	4,47E-21
325	2	12	7,28E-21	3,06E-21

330	5	11	1,86E-20	2,10E-21
335	8	8	2,97E-20	1,44E-21
340	11	11	4,38E-20	9,86E-22
345	5	9	1,83E-20	6,76E-22
350	4	9	1,36E-20	4,63E-22
355	10	9	3,86E-20	3,17E-22
360	4	8	1,34E-20	2,18E-22
365	3	10	1,14E-20	1,49E-22
370	0	7	-1,79E-21	1,02E-22
375	6	7	2,27E-20	7,00E-23
380	6	7	2,27E-20	4,80E-23
385	7	7	2,55E-20	3,29E-23
390	6	7	2,27E-20	2,25E-23
395	-2	9	-7,82E-21	1,55E-23
400	1	8	4,07E-21	1,06E-23

[a]Wavelength in *nm*, Molar Absorptivity in *L mol^{-1} cm^{-1}* and cross section values in cm^2 molec^{-1}
[b]Extrapolated cross section from 290 to 400 nm (see text)

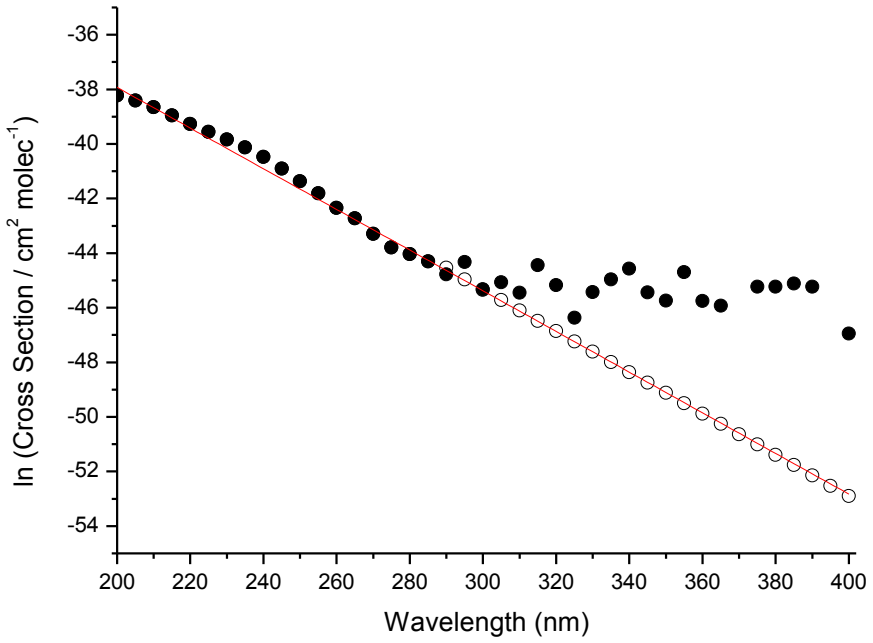

Figure S4. Natural Logarithm of the cross section of NH_4IO_3 vs wavelength. Fill black circles are the measured values, red line is the linear fit of these points in the interval 200-290 nm, and open black circles are the extrapolated values, using the fitting line, in the 290-400 nm interval.

6. Calculation of an Action Spectrum

In order to have a realistic estimation of the wavelength range relevant in our photolysis process, we have calculated an action spectrum, defined as a product of the IO_3^- cross section and the % transmittance of the glass window and the lamp output. This spectrum is shown in Figure S5 (upper panel), and it shows null absorption values below 250 nm, due to the transmittance of the glass window is zero in this range. The spectrum shows a maximum around 290 nm, and it decreases ca. 1000 times at 400 nm.

In addition, in Figure S5 (lower panel), we show an action spectrum at the Antarctic conditions (October at 75° S latitude). We have used the calculated IO_3^- cross section and the photon flux at the Antarctic sunlight. It is evident in the Figure that action spectrum in Antarctic conditions is around 6 times lower than during the experiments. The reason is that photon flux under Antarctic conditions is also ca. 6 times lower.

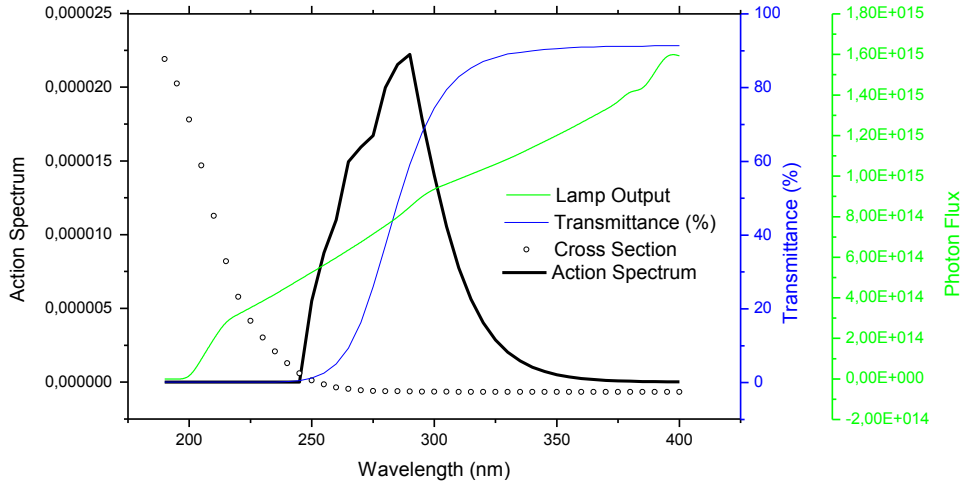

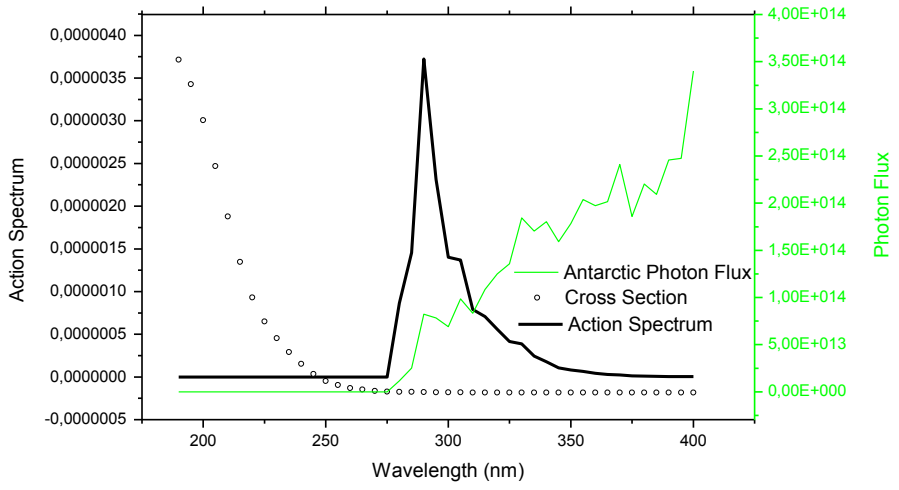

Figure S5. Upper panel: Action Spectrum in the experiments (defined as a product of the IO_3^- cross section and the % transmittance of the glass window and the photon flux provided by the lamp). Lower panel: Action spectrum at Antarctic sunlight conditions (defined as a product of the IO_3^- cross section and Antarctic sunlight photon flux).

REFERENCES

Houghton, J.: The Physics of Atmospheres, Cambridge University Press, 2002.
Twardowski, M. S., Boss, E., Sullivan, J. M., and Donaghay, P. L.: Modeling the spectral shape of absorption by chromophoric dissolved organic matter, Marine Chemistry, 89, 69-88, http://dx.doi.org/10.1016/j.marchem.2004.02.008, 2004.